ACS APPLIED MATERIALS & INTERFACES

Research Article

www.acsami.org

Green Synthetic, Multifunctional Hybrid Micelles with Shell Embedded Magnetic Nanoparticles for Theranostic Applications

Yongyong Li,*[,†] Junping Ma,[†] Haiyan Zhu,[†] Xiaolong Gao,[‡] Haiqing Dong,[†] and Donglu Shi[§]

[†]The Institute for Biomedical Engineering and Nano Science, Tongji University, Shanghai 200092, P.R. China

[§]Materials Science and Engineering Program, University of Cincinnati, Cincinnati, Ohio 10 45221, United States

[‡]Department of Medical Imaging, Tongji Hospital, Tongji University, Shanghai 200065, P.R. China

ABSTRACT: The objective of this study is to design and develop a green-synthetic, multifunctional hybrid micelles with shell embedded magnetic nanoparticles for theranostic applications. The hybrid micelles were engineered based on complex micelles self-assembled from amphiphilic block copolymers Pluronic F127 and peptide-amphiphile (PA) pal-AAAAHHHD. The reason to choose PA is due to its amphiphilic character and the coordination capability for Fe^{3+} and Fe^{2+}. The PA incorporation allows the in situ growth of the magnetic iron oxide nanoparticles onto the complex micelles, to yield the nanostructures with shell embedded magnetic nanoparticles at an ambient condition without any organic solvents. The anticancer drug doxorubicin (DOX) can be efficiently loaded into the hybrid micelles. Interestingly, the magnetic nanoparticles anchored on the shell were found to significantly retard the DOX release behavior of the drug loaded hybrid micelles. It was proposed that a cross-linking effect of the shell by magnetic nanoparticles is a key to underlie the above intriguing phenomenon, which could enhance the stability and control the drug diffusion of the hybrid micelles. Importantly, in vitro and in vivo magnetic resonance imaging (MRI) revealed the potential of these hybrid micelles to be served as a T_2-weighted MR imaging contrast enhancer for clinical diagnosis.

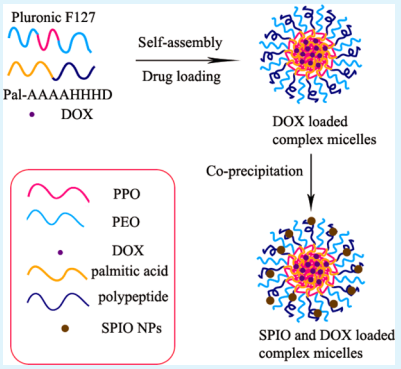

KEYWORDS: *green synthesis, multifunction, hybrid micelles, MR imaging, theranostic*

1. INTRODUCTION

Nanoscience has been playing a significant and rapidly evolved role in molecular diagnostics, tissue engineering, precise imaging, and improved therapeutic effect.[1,2] Recently, the emerging concept of "theranostic", defined by simultaneous therapeutic and diagnostic functions in one system, is a promising strategy that may generate significant influence on biomedical applications, especially personalized medicine. From the therapeutic aspect, theranostic nanosystem enables the effective localization of the therapeutic agent within a tumor and subsequently leads to improved treatment effect.[3−5] The enhanced therapeutic effect has been generally achieved by the prolonged circulation time, protection of the degradation of the entrapped payload prior to the action, and increased tumor uptake associated with well-known EPR effect, as well as the potential targeting capability mediated by the overexpressing of the receptor in tumor microenvironment.[6,7] Furthermore, diversiform therapeutic agents such as antineoplastic, anti-angiogenic, or gene agents can be collectively encapsulated and navigated toward disease sites aided by one nanosystem to improve the therapeutic index.[8,9] From the aspect of diagnosis, imaging agents can be further carried with therapeutical agents into one nanosystem with tumor-specific markers, enabling to differentiate the tumors from normal tissues as well as to enable seamless integration of diagnosis, treatment and monitoring.[10−13]

Polymeric micelles represent nanoparticles self-assembled from various amphiphilic block copolymers. These unique nanomaterials have received considerable attention for biomedical applications.[14−16] Polymeric micelles have been shown to exhibit excellent biocompatibility, high drug-carrying capability, and physiological stability.[17] Low critical micellar concentration (CMC) of polymeric micelles provides the stability in solution compared with conventional liposome.[18] On the other hand, the homogeneous nanoparticles can effectively hinder the fast exclusion by renal route and the reticulo-endothelial system (RES) system, while enhancing permeability and retention.[19,20] However, it has been a great challenge to achieve "theranostics" via polymeric micelles because of complicated or toxic chemical processes required to incorporate imaging agents in a single-copolymer-based micellar system. As a result, there have been a few reports on micelle-based "theranostic" system, as most of the previous works are extensively focused on drug storage for therapeutics.[21]

Complex micelles that are self-assembled from two or more structurally different amphiphilic copolymers can be a practical and efficient strategy to address this critical issue described above.[22−24] Different block copolymers can be designed and

Received: April 27, 2013
Accepted: July 1, 2013
Published: July 1, 2013

mixed with respective function to make a "multifunctional" system.[25,26] The multifunctionalilty can be engineered into theranostic nanosystem for drug delivery, controlled release, and medical diagnosis etc.[27−29] Liu et al.[30] reported on the utilization of complex diblock copolymer micelles coassembled from PCL-b-P (OEGMA-FA) and PCL-b-P (OEGMA-Gd) as an integrated multifunctional scaffold for combined MRI contrast enhancement and targeted chemotherapeutic drug delivery. Their preliminary results indicated complex micellar nanocarriers with synergistically integrated functions of cancer-targeted drug delivery, controlled release, and MR imaging contrast enhancement.

In this study, we present a green-synthesis of hybrid micelles with the shell-embedded magnetic iron nanoparticles for theranostic applications, in contrast to the traditional magnetic nanoparticles that were generally encapsulated in the micellar core. The hybrid micelles are integrated with functions of therapeutical effect and MR imaging. The complex micelles were fabricated from Pluronic F127 and peptide-amphiphile (PA) pal-AAAAHHHD. The formation of the complex micelles was driven by the hydrophobic interaction between hydrophobic segments of Pluronic F127 and PA, encapsulating hydrophobic drug DOX. The in situ growth of magnetic nanoparticles in the shell of the complex micelles was further achieved by chemical precipitation of $FeCl_3$ and $FeCl_2$ for generation of the hybrid micelles with the shell-embedded magnetic iron nanoparticles. The formation of drug-loaded hybrid micelles is within two steps at an ambient condition without any organic solvents and vast energy input. The entire procedures are fast, efficient, and convenient. The hybrid complex micelles further exhibit significantly improved stability with favorably retarded and controlled drug release, due to the cross-linking effect of the magnetic nanoparticles among the shell. Furthermore, the hybrid micelles have shown an interesting T_2-weighted MR imaging capability, suggesting the potential for theranositic applications.

2. EXPERIMENTAL SECTION

Materials. Pluronic F127 were obtained from sigma-Aldrich (Shanghai, China) and used as received. Peptide-amphiphile (PA) pal-AAAAHHHD was purchased from GL Biochem, Ltd. The mass spectrum provided by the supplier supports the desired structure. Doxorubicin hydrochloride (DOX·HCl) were purchased from Beijing United Technology CO., Ltd. and used as received. Iron(III) chloride hexahydrate ($FeCl_3{\cdot}6H_2O$) and iron(II) chloride tetrahydrate ($FeCl_2{\cdot}4H_2O$) were purchased from Sinopharm Chemical Reagent Co., Ltd. (SCRC, Shanghai, China) and used as received. Dulbecco's modified Eagle's medium (DMEM), trypsin, Dubelcco's phosphate buffered saline (DPBS), 3-(4,5-dimethylthiazol-2-yl)-2,5-diphenyltetrazolium bromide (MTT), fetal bovine serum (FBS), penicillin-streptomycin were obtained from Gibco Invitrogen Corp. 2-(4-Amidinophenyl)-6-indolecarbamidine dihydrochloride (DAPI) was purchased from Beyotime Institute of Biotechnology. The dialysis bags (Spectra/Por 7) were obtained from Spectrum Laboratories Inc.

Self-Assembly of Complex Micelles. In a typical protocol, 8.0 mg of Pluronic F127, 2.0 mg of PA, and 3.0 mg of DOX·HCl were dissolved in 5.0 mL of deionized water through sonication. Twenty microliters of triethylamine was subsequently added to desalinate DOX·HCl. The sonication continued for 30 min. Complex micelles were then generated after a heating at 80 °C for 10 min under vigorous stirring. The formation of micelles was confirmed by the appearance of a very light-blue solution, which is the characteristic of micelles formation. Dynamic light scattering (DLS) was carried out to measure the overall size and size distribution. The residual DOX was removed by a dialysis process against the membrane with MWCO (molecular weight cut-off) of 3500.

Preparation of DOX-Loaded Hybrid Micelles. The hybrid micelles were prepared by chemical precipitation of Fe_3O_4. Briefly, the aqueous solution of $FeCl_3{\cdot}6H_2O$ (4.1 mg) and $FeCl_2{\cdot}4H_2O$ (2.0 mg) (in a 1.5:1 molar ratio) was purged with Argon for 30 min. Then it was added dropwise to the aqueous suspensions of DOX loaded complex micelles that generated in the above process. The mixture was stirred vigorously under Argon protection for ion interaction, and then the pH of suspensions was adjusted to pH 10 by mildly exposing the solution to NH_3 vapor (from concentrated NH_4OH) and the temperature was elevated to 60 °C gradually. The NH_3 exposure allowed the occurrence of the precipitation of Fe_3O_4, to yield the hybrid micelles.

In Vitro Drug Release Study. In vitro drug release from the DOX loaded complex micelles and hybrid micelles were assessed in PBS (pH 7.4) at 37 °C. Drug-loading capacity for DOX in complex micelles was quantified by using a UV−vis spectrophotometer (UV759S, Q/YXL270) to compare the absorbance of this solution at 480 nm with a calibration curve of aqueous DOX solutions with known concentration. Drug-loading capacity of DOX in DOX-loaded hybrid micelles is calculated as percentage of total DOX added according to

$$\text{drug loading capacity}\ (\%) = (M_0/M_a)100\%$$

$$\text{cumulative DOX release}\ (\%) = (M_t/M_0) \times 100\%$$

Where M_a is the weight of micellar materials added, M_t is the total amount of DOX released from the micelles at time t, and M_0 is the amount of DOX initially loaded into the micelles.

In Vitro and In Vivo MRI Characterization. The protocol was followed as the reported work.[29] For in vitro MRI assessment of magnetic hybrid micelles, T_2 was obtained by using a 3.0 T MR scanner. The T_2-weighted signals were acquired via the method of spin echo acquisition (TR = 4000 ms). The MRI effects of magnetic micelles were evaluated in nude mice. For in vivo MRI, female nude mice (~20 mg) were subjected to in vivo MRI assessment. MRI images of nude mice were acquired. The hybrid micelles with the predetermined amount were injected into the tumor bearing nude mice via the tail vein. Images were collected at different time intervals post injection of micelles. Images were also obtained at preinjection as a control. The relative signal intensities at preinjection and postinjection in the region of interest (ROI) were recorded for analysis.

Cytotoxicity Test. The cytotoxicity of the complex micelles, DOX loaded complex micelles and DOX loaded hybrid micelles against HeLa cells were investigated by measuring the cell viabilities using the conventional MTT assay. First, HeLa cells were seeded into a 96-well plate at a density of 5000 cells/well and subject to overnight incubation with DMEM at 37 °C exposed to a humidified 5% CO_2 atmosphere. These cells were then interacted with hybrid micelles with different concentrations range from 58 mg/L to 1000 mg/L for 12 and 24 h. Thereafter, the cell culture medium in each well was changed with 100 μL of fresh medium and the cells were allowed a 4 h incubation with 20 μL of sterile filtered 3(4,5dimethylthiazol2yl)2,5-diphenyltetrazolium bromide (MTT, 5 mg/mL) in warm PBS. After the removal of the culture medium, DMSO (100 μL) was replenished into each well which was kept for 10 min on a shaking platform at 25 °C. The absorbance of the resulting solution was measured at 570 nm using a Multiscan MK3 plate reader. The cell viability was calculated according to the ratio of the intensity of purple formazan in viable cells treated with hybrid micelles to that of the untreated control cells.

Cellular Uptake Study. Confocal laser scanning microscopy (CLSM) was applied to assess the behaviors of cellular uptake and intracellular release of DOX-loaded hybrid micelles by using HeLa cell as the model. Hela cells were incubated with DOX-loaded hybrid micelles for different hours exposed to a humidified 5% CO_2 atmosphere at 37 °C. After the removal of the culture medium of the wells, the cells were thoroughly rinsed with PBS before the microscopic observation. Upon observation, the cells were fixed with

the cell nuclei being stained with 2-(4-amidinophenyl)-6-indolecarbamidine dihydrochloride (DAPI, blue). CLSM images were acquired by using confocal microscope (TCS SP2).

Characterization. DLS studies of aqueous polymer complex micelles and magnetic hybrid micelles solutions were determined using NanoZS 90 Nanosizer (Malvern Instruments Ltd., Worcestershire, UK) with the scattering angle fixed at 90°.

Transmission electron microscopy (TEM) images were acquired by H7100 electron microscope with an acceleration voltage of 100 kV. For the preparation of TEM samples, placing a drop (5 μL) of the resultant solution on a holey carbon-coated copper grid and wicking the drop through the back side of the grid with filter paper.

TGA characterizations were followed as the reported work.[31] It was performed by using a PEPKIN ELMER thermal gravimetric. The temperature was kept from room temperature to 1000 °C in N_2 flow at a specific heating rate.

The crystallographic data of the samples were characterized by X-ray diffraction (XRD, D/MAX-IIIC, Japan). The XRD patterns were obtained from 10 to 90° (2θ) based on Cu Kα radiation at a predetermined scanning rate.

UV−vis tests were followed as the reported work.[31] They were performed by using an UV−vis spectrophotometer (UV759S, Q/YXL270, SHANGHAI PRECISION & SCIENTIFIC INSTRUMENT CO., LTD). The absorbance spectra of the hybrid micelles were collected within the range of 200−800 nm wavelengths.

The in vivo MRI assessment was characterized by using a 3.0 T MR scanner (Verio, Siemens, Munich, Germany) at 25 °C. The relaxometry was performed using a 1.4 T minispec mq60 NMR Analyzer (Bruker, Germany) followed with the reported protocol.[32] The micelles were suspended at the Fe concentrations between 0.0005 and 0.04 mM for characterization.

3. RESULTS AND DISCUSSION

Basic Considerations for the Copolymer Selection. Complex micelles are engineered from two amphiphilic copolymers including Pluronic F127 and PA. Pluronic F127[33] is a copolymer well-known for its biocompatibility, consisting of poly (ethylene oxide) and poly (propylene oxide) blocks with structural parameters of PEO_{100}-PPO_{65}-PEO_{100}.[34,35] The rational for the biomedical use of Pluronic F127 relies on its amphiphilic nature with a relatively short hydrophobic PPO chain flanked by two long hydrophilic PEO chains. The exterior PEO functions as an antifouling characteristic to avoid the occurrence of self-aggregation, resistance of the protein conglutination, and RES sequestration, whereas the hydrophobic PPO located in the middle of the structure can be harnessed to carry the anticancer agents with the hydrophobic property.[36,37] Micelle formulations based on Pluronic F127 usually show a low stability (usually appeared as high critical micelle concentration) especially when subjected to dilution, because of the high ratio of hydrophilic/hydrophobic segment. The fabrication of multifunctional Pluronic F127-based micelles is a complex process as the terminal groups are not effective for modification at ambient condition. Complex micelles represent a feasible route to address this challenge by incorporating other amphiphilic polymers into Pluronic F127 micelles.

PA consisting of segments of palmitic part, aspartic acid residue and three histidine amino acids is chosen to cooperate with Pluronic F127 to develop the complex micelles (Figure 1). Different segments play specific roles. Palmitic part is the essential hydrophobic segment for micelles assembly. Segments of aspartic acid residue and histidine amino acids provide the function of chelating with Fe^{2+} or Fe^{3+} to deposit Fe_3O_4 nanoparticles. Specifically, histidine is known to chelate Fe^{2+}, driven by the coordination capability via the δ-nitrogen with the lone electron pair. It is reported that the relatively low pK_a of

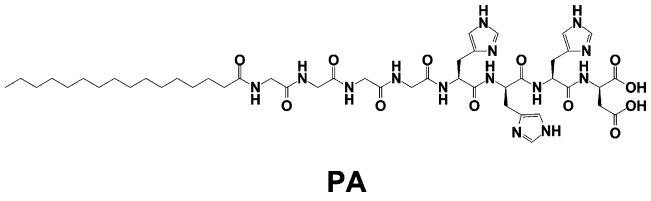

Figure 1. Chemical structure of peptide-amphiphile (PA) pal-AAAAHHHD.

histidine (6.0) would result in a predominant deprotonated δ-nitrogen at the pH where Fe(II) is kept soluble, thus leading to the occurrence of ion coordination.[38] Meanwhile, aspartic acid residue containing additional two free carboxyl groups can coordinate with Fe^{3+}.[38] Despite the amphiphilic nature of the lipid peptide, the structure of PA is not favorable to form micelles because of its relatively high ratio of hydrophobic to hydrophilic segment. However, for an optimum hydrophilic/hydrophobic ratio, the structure of PA is favorable to self-assembly with Pluronic F127 to form complex micelles.

Self-Assembly of Complex Micelles. The experimental design of the complex micelles is illustrated in Scheme 1.

Scheme 1. Schematic Illustration of the Process to Yield Multifunctional Hybrid Micelles

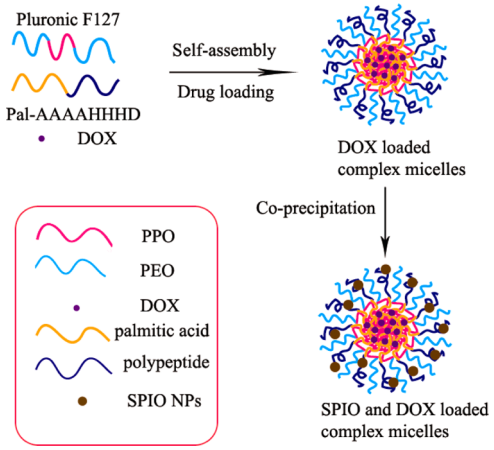

Pluronic F127 and PA self-assemble into complex micelles by directly dissolving both of them in aqueous solution under sonication. The process of the self-assembly is driven by hydrophobic interaction between the hydrophobic segment of the two copolymers. DOX can be simultaneously encapsulated into the complex micelles either by hydrophobic interaction after a desalination treatment of DOX·HCl by triethylamine. The as-formed complex micelles feature a core−shell structure with the functional peptide distributing in the shell. Taking advantages of chelating capabilities of the peptide, the magnetic nanoparticles can be generated in situ within the shell of the complex micelles by chemical precipitation of $FeCl_3$ and $FeCl_2$ solution. In this route, hybrid micelles are developed with shell-embedded magnetic nanoparticles.

The entire process was carried out under an ambient condition without incorporating any organic solvents. This implies an environmentally benign green synthesis of the hybrid micelles. The magnetic nanoparticles are embedded in the shell of the as-formed hybrid micelles, which is advantageous compared to the conventional synthesis of the magnetic

polymeric nanosystems in which the magnetic nanoparticles must be subsequently incorporated in the core.

Three complex micelles with different feed ratios (Table 1) of Pluronic F127 were fabricated. In the assembly of the complex micelles, Pluronic F127 alone cannot self-assemble into stable micelles, as confirmed by the statistic data of DLS. However, the improved stability of complex micelles by PA incorporation is evident when incorporating a relatively low ratio of PA into the complex micelles. Uniform and sub-100 nm micelles were observed for micelles with three different feed ratios. The micelles stability is evidently improved by changing the micelles structure. As shown in Table 1, complex micelles 2 are uniform for most of the homogeneous sizes that found unchanged for 1 month. Thus, complex micelles 2 are chosen for the following experiments.

Table 1. Size and PDI of the Complex Micelles with Different Compositions Determined by DLS at 25 °C

	composition			
complex micelles	Pluronic F127(mg)	PA (mg)	*d* (nm)	PDI
1	9	1	73 ± 3.5	0.19
2	8	2	56 ± 3.9	0.14
3	7	3	69 ± 6.4	0.28

^{1}H NMR analysis was investigated to study the formation of the complex micelles (Figure 2). The peaks at 3.53 and at 1.0 ppm are respectively assigned to $-CH_2$ in PEO and $-CH_3$ in PPO in the backbone of Pluronic F127. Those from 4.0 to 9.0 ppm belong to the repeating units of the histidines and aspartic acid, respectively. As expected, the peaks of Pluronic F127 and PA are both observed in the spectrum of the complex micelles and vary at different compositions, which indicate the formation of the complex micelles. Further observation by TEM shows a regular spherical and uniform morphology of the complex micelles with the size smaller than that observed in DLS study. The typical TEM images, as shown in Figure 3a, show that the complex micelles with a diameter around 40 nm, while DLS measurements indicate an average size of 60 nm in diameter (Figure 3c). The difference originates from the shrinking effect of the complex micelles from hydrate to dried state in the TEM and DLS experiments.

Fabrication and Structural Characterization of Hybrid Micelles. The broad applications of hybrid nanoparticles have been generally hampered by their multiple synthesis steps. Herein, hybrid micelles were fabricated in two steps without detrimental organic solvent and large quantity of energy input. The engineering of organic/inorganic hybrid micelles were based on the uniform and stable complex micelles 2. It is well documented that DOX as a hydrophobic anticancer drug can be effectively loaded into the hydrophobic micellar cores driven by hydrophobic interaction. Protected and stabilized by the micellar nanocarriers, controlled drug release can be achieved. PA in the complex micelles exhibits high affinity with Fe atoms, and complex micelles can function as potent stabilizing protection to the carried magnetic nanoparticles. The hybrid micelles were then prepared by in situ chemical precipitation of iron oxides in the shell of complex micelles. The molar ratio of Fe^{3+}/Fe^{2+} concentrations is optimized to be at 1.5:1 to chelate with carboxylate anions and histidines on the surface of complex micelles. The solution was stirred vigorously under argon protection for ion exchange, and the suspensions were then exposed to NH_3 vapor (from concentrated NH_4OH) to afford hybrid micelles.

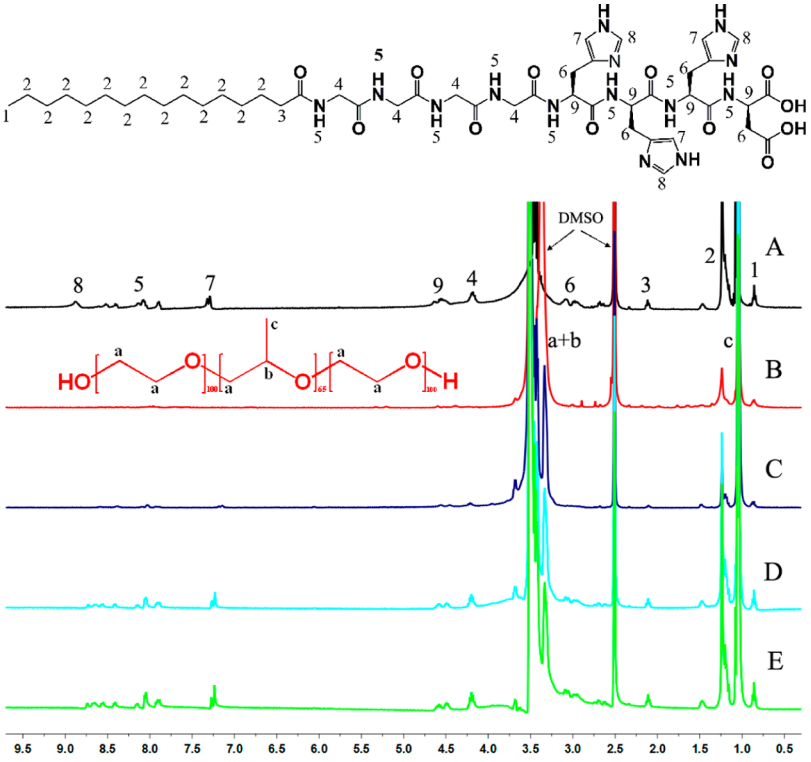

Figure 2. ^{1}H NMR spectra of (A) peptide-amphiphile (PA) pal-AAAAHHHD in DMSO-d6; (B) Pluronic F127. ^{1}H NMR spectra of complex micelles with different composition: (C) complex micelles 1; (D) complex micelles 2; (E) complex micelles 3 in DMSO-d_6. The compositions of complex micelles refer to Table 1.

dx.doi.org/10.1021/am401573b | ACS Appl. Mater. Interfaces 2013, 5, 7227−7235

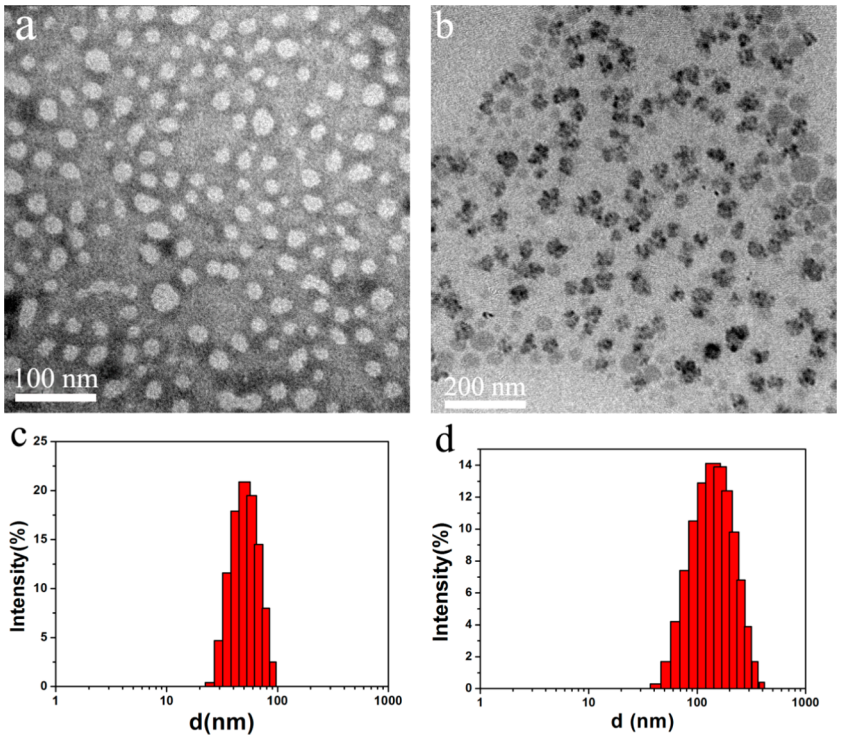

Figure 3. TEM images of (a) complex micelles 2 and (b) hybrid micelles. Size distributions of (c) complex micelles, and (d) hybrid micelles in water.

Upon the chemical precipitation process, Fe_3O_4 nanoparticle can be successfully deposited onto the shell of the complex micelles. The TEM observation (Figure 3b) shows a clear core−shell structure with some of the dark spots distributing throughout the shell. These dark spots are associated with the Fe_3O_4 nanoparticles with a higher contrast than copolymers. The size of the Fe_3O_4 nanoparticles was estimated to be ∼10 nm though some of them appears as aggregated state. As shown in Figure 3b, the typical image of the hybrid micelles shows an increased size to 60 nm compared with complex micelles at around 40 nm (Figure 3a). The hydrodynamic size of the hybrid micelles determined by DLS is about 130 nm, which is larger than that observed under TEM, because of the removal of water during TEM sample preparation.

The structure of the hybrid micelles was studied by X-ray powder diffraction. As shown in Figure 4, the main peaks at 2θ of 27, 32, 45, 57, 66, 75, and 84° correspond, respectively, to the (220), (311), (400), (511), (440), (531), and (533) planes of the face-centered cubic (fcc) Fe_3O_4 crystal structure.[11] These characteristics are fingerprint characteristics of Fe_3O_4 crystal, indicating the presence of Fe_3O_4 nanoparticles. In contrast, three broad peaks can be found in the complex micelles because of poor crystallinity of copolymers.

TGA studies of the complex micelles and hybrid micelles were carried out under nitrogen atmosphere. As shown in Figure 5 at temperatures below 100 °C, a small weight loss is attributed to the vaporization of residual or absorbed solvent. Then a stage of large weight loss occurs around 420 °C, indicating the decomposition and gasification of water and the high-molecular-weight polymer. The small weight loss at 600 °C is attributed to the breakdown of the −COO group coordinated with Fe_3O_4 nanoparticles in the magnetic vesicles. There is no obvious weight loss occurred above 750 °C with residual mass percentages of 5.86% (complex micelles) and

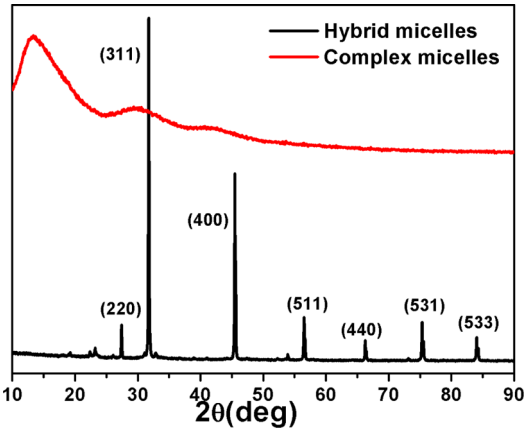

Figure 4. X-ray powder diffraction patterns of complex micelles and hybrid micelles.

23.77% (hybrid micelles). Obviously, the weight losses of different stages are associated with the relative content of the different compositions of the hybrid micelles. The Fe_3O_4 content of the hybrid micelles is calculated to be approximately 18 wt % from the TGA data.

Stability and Magnetic Property of Hybrid Micelles. The effect of Fe_3O_4 nanoparticles on the stability was studied. The size variation of the hybrid micelles upon dilution was evaluated by using DLS. The size alteration of the complex micelles was also monitored as the control experiment. Generally, size alteration upon dilution is a good indication of stability. In the assay, three orders of dilution were used corresponding to the concentration from 1 to 0.001 mg/L. The sizes at different concentrations for both complex and hybrid micelles were monitored. As shown in the Table 2, neglectable alterations of size are observed when subjected to dilution from

dx.doi.org/10.1021/am401573b | ACS Appl. Mater. Interfaces 2013, 5, 7227−7235

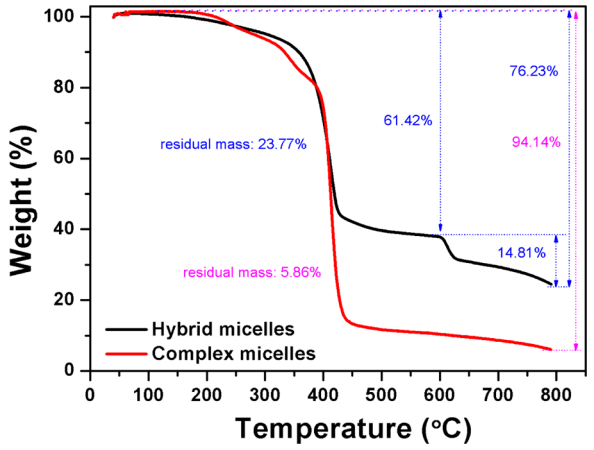

Figure 5. TGA curves of complex micelles and hybrid micelles.

Table 2. Dilution Resistance of Complex Micelles and Hybrid Micelles[a]

C (mg/L)	1	0.1	0.01	0.001
d_1 (nm)	60	65	140	320
d_2 (nm)	140	140	210	290

[a] d_1, d_2 are the size of complex micelles and hybrid micelles respectively.

1 to 0.1 mg/mL for both complex and hybrid micelles. As the concentration decreases to 0.01 mg/L, a moderate size increase appears for hybrid micelles from 140 to around 200 nm, whereas size doubles from 65 to 140 nm for complex micelles. The size of complex micelles at 0.001 mg/L further increases significantly by five times (320 nm). However, at the same concentration, the hybrid micelles only exhibit a moderate size increase. These results show that incorporation of Fe_3O_4 nanoparticles into complex micelles has stabilized the system. The stabilization is associated with the shell cross-linking effect of Fe_3O_4 nanoparticles distributed throughout the shell. On the basis of the above uniform and stable complex micelles 2, Fe_3O_4 nanoparticles can simultaneously coordinate with several PA molecules and act as the cross-linking site.

Because of the incorporated Fe_3O_4 nanoparticles, the hybrid micelles are expected to be regulated by an external magnetic field. Figure 6 (up panel) presents the hybrid micelles dispersed in aqueous solution and that of micelles subject to an external magnetic field. Without external magnetic field, the solution of the hybrid micelles is brown-colored homogeneous suspension. Upon application of the magnetic field, these hybrid micelles respond to it by migrating toward the magnet. This process is reversible. After the removal of the external magnetic field, the aggregates can be rapidly redispersed by gentle shaking.

In Vitro MR Imaging. MRI is known as one of the most effective noninvasive method at present for medical imaging to analyze the pathological alterations of tissues.[39] It outweighs other methodologies because of its several advantages for clinical benefits.[40] Magnetic iron oxide nanoparticles as a promising contrast agent was known to be capable of shortening the transverse relaxation time of water protons and thus could be applied for MR imaging.[41] With respect to the unique structure of the hybrid micelles with shell-embedded magnetic iron nanoparticles, the in vitro MRI effect of the hybrid micelles was investigated. T_2-weighted MR images of hybrid micelles with an increased iron concentration are

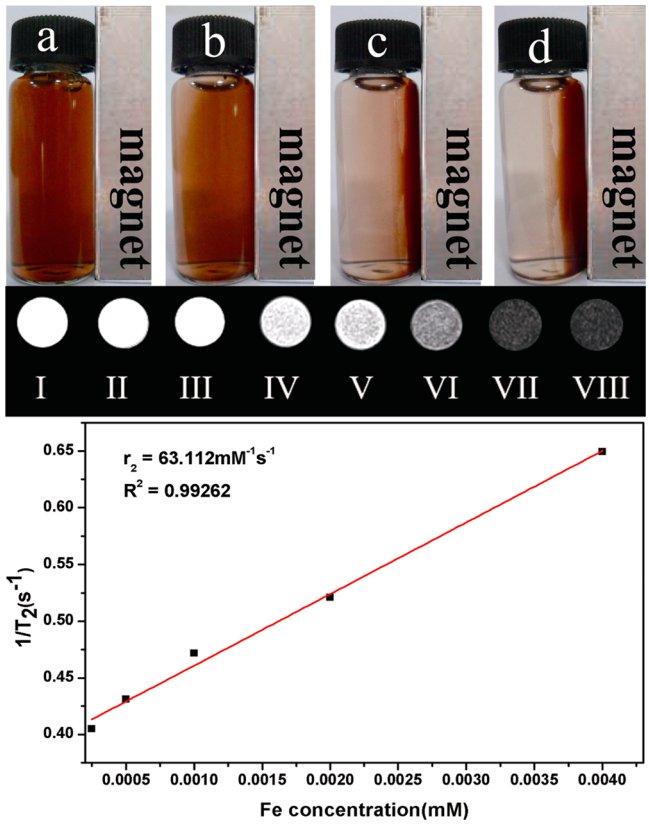

Figure 6. Macroscopic view (up panel) of magnetic complex micelles from 0 to 72 h in an external magnetic field: (a) 0, (b) 6, (c) 24, (d) 72 h. T_2-weighted MR images (middle panel) of magnetic complex micelles: (I) H_2O; (II) complex micelles; (III) complex micelles; hybrid micelles: (IV) Fe concentration 0.5 μM; (V) Fe concentration 1 μM; (VI) Fe concentration 2 μM; (VII) Fe concentration 4 μM; (VIII) Fe concentration 8 μM. T_2 relaxation rate ($1/T_2$) (bottom panel) as a function of Fe concentration recorded for the aqueous solution (37 °C) of hybrid micelles.

obtained by one clinical 3T MRI apparatus. As shown in Figure 6 (middle panel), MR images of the hybrid micelles dispersed in aqueous solution display darkened contrast as a function of the increased concentration. In contrast, the medium without magnetic oxide nanoparticles presents no contrast without shadows. The decreased intensity is more pronounced at the higher concentration indicating that these hybrid micelles could be applied as the contrast of negative enhancement (darkened signal) in MRI. The relaxation rates of the hybrid micelles (bottom panel, Figure 6) increase linearly with the concentration of hybrid micelles. The data yield an r_2 of the hybrid micelles at around 63.112 mM^{-1} s^{-1}.

In Vitro Drug Release. To assess the potential of hybrid micelles for drug delivery application, we encapsulated a hydrophobic model drug, DOX, and investigated in vitro drug release of the DOX-loaded hybrid micelles in PBS (pH 7.4) at 37 °C. Hydrophobic interaction between DOX and hydrophobic core of the hybrid micelles was believed to drive the loading process, with the drug loading content of 21.5 wt % calculated according to the procedure described in the experimental part. The incorporation of PA into the hybrid micelles was believed to contribute the fact of the relatively high DOX loading efficiency. The in vitro DOX release behavior in PBS (pH 7.4) at 37 °C is investigated respectively for DOX-loaded complex micelles and hybrid micelles. A

different in vitro behavior of drug release is observed due to the cross-linking effect of the magnetic nanoparticles that impedes the diffusion of the encapsulated drug into the medium. The in vitro DOX release of hybrid micelles was investigated for different Fe concentrations. As shown in Figure 7, DOX release

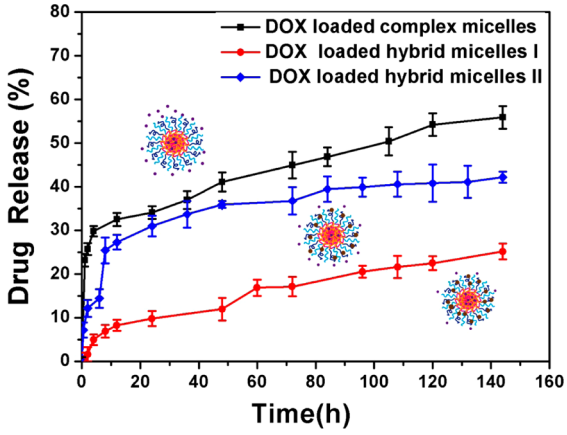

Figure 7. Release behavior of DOX from DOX-loaded complex micelles and hybrid micelles in PBS at 37 °C. Hybrid micelles II are 50% Fe concentration compared with hybrid micelles I.

from the complex micelles display a typical behavior similar to other drug loaded micelles. There shows a rapid release at initial 10 h (30% drug release), followed by a slowdown up to 120 h. In contrast to the complex micelles, hybrid micelles with shell-embedded magnetic nanoparticles show a retarded drug release, especially for high Fe concentrations (hybrid micelles I). Remarkably, DOX release from the hybrid micelles I exhibits a gradual release, no more than 7% at the first 10 h, then a near linear release. The release of the hybrid micelles (15%) is remarkably lower than that of the complex micelles (55%). This is clear evidence of release suppression due to the incorporation of the magnetic nanoparticles. In this regard, the near linear release is achieved for a favorable drug delivery. Additionally, it should be noted that the DOX release behavior is Fe concentration dependent. Hybrid micelles I with lower Fe concentration does not show obvious effect of the controlled drug release.

Cytotoxicity Study. The therapeutic efficacy of the DOX-loaded hybrid micelles was evaluated in vitro by quantifying cell viability of HeLa cancer cells by the conventional MTT assay. HeLa cells were incubated with the complex micelles, DOX-loaded complex micelles, and DOX-loaded hybrid micelles at different concentrations. As shown in Figure 8, as an important control experiment, the complex micelles without DOX do not obviously affect the cell viability of this cell line even at a high concentration of 1 mg/mL, and the high concentration of complex micelles boost cell proliferation compared with some of the low concentrations. To assess the curative effect of DOX loaded complex/hybrid micelles, we evaluated cytotoxicity of DOX-loaded micelles against HeLa cells. Cell viability of HeLa cells decreases as a function of the micelles concentration for both complex and hybrid formulations. Different time of culture for either 12 or 24 h was chosen to assess the retarded DOX release of the hybrid micelles on cell viability. A more potent cytotoxicity is found for extending the time to 24 h especially for high concentrations, suggesting the retarded release of DOX in line with the result of in vitro drug release assay. Note that the cell viability of DOX-loaded hybrid micelles is higher than DOX-loaded complex micelles, indicating faster release of DOX from the complex micelles.

Intracellular Uptake Behavior. The cellular uptake of DOX-loaded hybrid micelles was observed by CLSM using human HeLa cells incubated with different time periods (see Figure 9). DOX can be easily traced under CLSM due to its inherent red fluorescence. To assess the spatial distribution of DOX, we labeled the cell nucleus by DAPI with blue fluorescence. It is found that only after 0.5 h incubation with cells, DOX fluorescence can be detected inside the cell. As the incubation time increases, the fluorescence of DOX distributes spatially and becomes pronounced at 2 h. After 4 h of incubation, red fluorescence is observed throughout the entire cells, suggesting efficient delivery of DOX into cells interior.

In Vivo MR Imaging. The in vivo MR imaging data of the hybrid micelles are shown in Figure 10. HeLa cell line was subcutaneously injected into the middle back of mice to prepare tumor-bearing mice. Following the intravenous injection of hybrid micelles, the MR imaging of the mice was acquired at specific time points. The tumor site was indicated by white arrows. After injection of the hybrid micelles, some darkened areas on the T_2-weighted MR images are found within the tumor site. A recovery of the signal intensities were observed as an increase of the time (Figure 10). Specifically, at 30 min postinjection, it presents lower relative signal intensity. Afterward, the gradual enhanced signal intensity appears. After 4 h, the relative signal intensity within the tumor site almost restores to the level of beginning of intravenous injection of hybrid micelles. The recovery of the signal intensity indicates

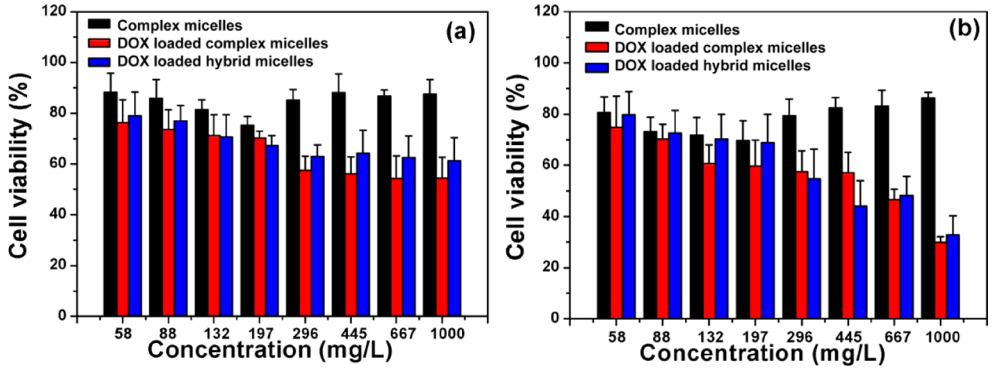

Figure 8. Cell proliferation of HeLa cells incubated with complex micelles, DOX-loaded complex micelles, and DOX-loaded hybrid micelles at various concentrations for the time periods indicated: (a) incubated for 12 h; (b) incubated for 24 h.

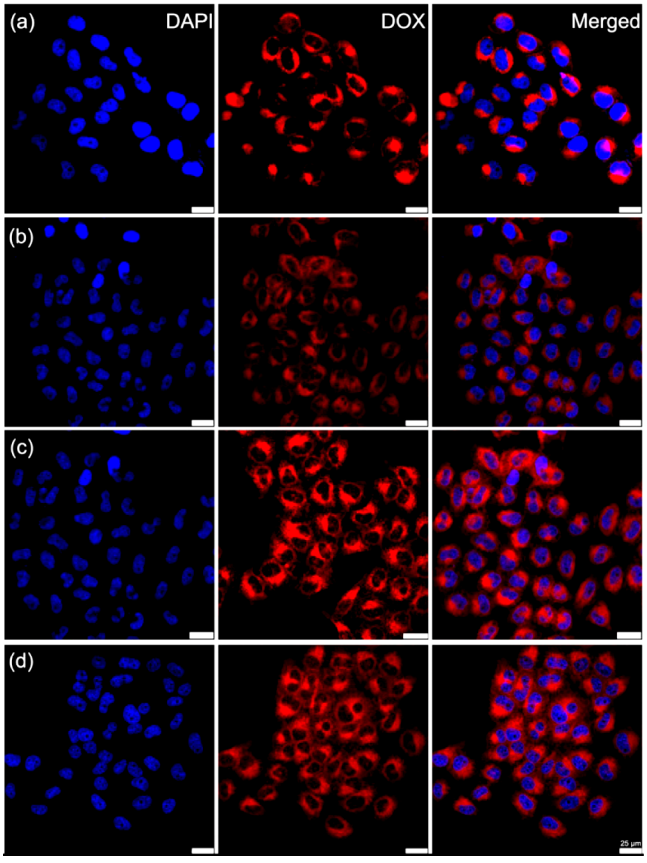

Figure 9. CLSM images of HeLa cells incubated with DOX-loaded hybrid micelles for different time periods: (a) 0.5, (b) 1, (c) 2, and (d) 4 h. Cell nuclei (blue) were stained with DAPI.

the excretion of the hybrid micelles within a moderate period, which is important to develop safe and efficient MR contrast agents without side effects, whereas enabling the effective diagnosis during theranostic application.

4. CONCLUSIONS

In this work, we have developed a novel multifunctional hybrid micelle with shell-embedded magnetic nanoparticles via a green synthesis route. The structure of the hybrid system is different from the traditional system where magnetic nanoparticles were generally encapsulated in the micellar core. The entire procedure of the synthesis in this work is fast, efficient, and convenient. The hybrid micelles are integrated with simultaneous drug delivery and MR imaging for theranostic applications. Magnetic oxide nanoparticles are successfully deposited onto the shell of the complex micelles, which are self-assembled by Pluronic F127 and PA. The magnetic nanoparticles anchored on the shell are found to significantly retard the DOX release of the drug loaded hybrid micelles. A cross-linking effect of the shell by magnetic nanoparticles is identified as the key for the enhancement of the stability and controlled drug release. Both in vitro and in vivo experiments show clear evidence that these hybrid micelles are potential alternatives for efficient MRI contrast agent and potential theranostic applications.

AUTHOR INFORMATION

Corresponding Author

*E-mail: yongyong_li@tongji.edu.cn. Tel.: +86-21-65983706. Fax: +86-21-65983706.

Notes

The authors declare no competing financial interest.

ACKNOWLEDGMENTS

This work was financially supported by 973 program (2013CB967500) and National Natural Science Foundation of China (51173136 and 21104059), Shanghai Rising-Star Program (12QA1403400), and "Chen Guang" project founded by Shanghai Municipal Education Commission and Shanghai Education Development Foundation.

REFERENCES

(1) Moghimi, S. M.; Hunter, A. C.; Murray, J. C. *FASEB J.* **2005**, *19* (3), 311−30.
(2) Leary, S. P.; Liu, C. Y.; Apuzzo, M. L. J. *Neurosurgery* **2006**, *58* (5), 805−823.
(3) Kelkar, S. S.; Reineke, T. M. *Bioconjugate Chem.* **2011**, *22* (10), 1879−1903.
(4) Sumer, B.; Gao, J. *Nanomedicine* **2008**, *3* (2), 137−40.
(5) Lammers, T.; Kiessling, F.; Hennink, W. E.; Storm, G. *Mol. Pharm.* **2010**, *7* (6), 1899−912.
(6) Peer, D.; Karp, J. M.; Hong, S.; FarokHzad, O. C.; Margalit, R.; Langer, R. *Nat. Nanotechnol.* **2007**, *2* (12), 751−760.

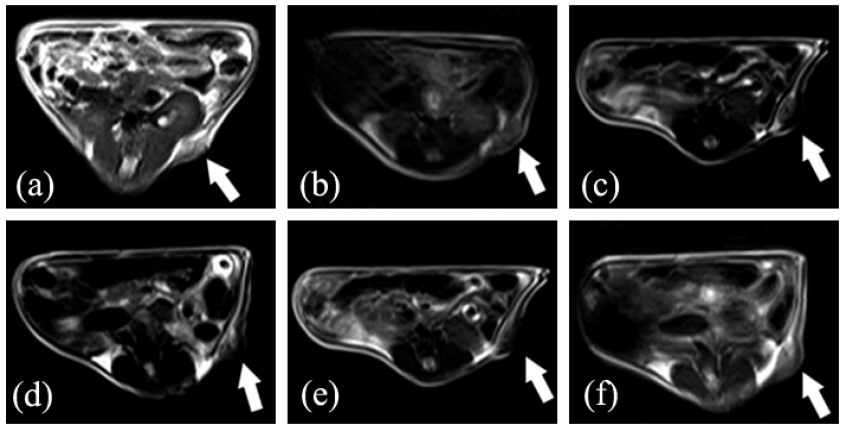

Figure 10. T_2-weighted MR images of the nude mice acquired (a) prior to and (b−f) post- injection of hybrid micelles whose hydrophilic shell embedded with magnetic oxide nanoparticles at different time periods: (b) 5 min, (c) 30 min, (d) 1 h, (e) 3 h, and (f) 4 h. The white arrows denote xenograft tumors.

(7) Park, J. H.; Lee, S.; Kim, J. H.; Park, K.; Kim, K.; Kwon, I. C. *Prog. Polym. Sci.* **2008**, *33* (1), 113−137.
(8) Fernandez-Fernandez, A.; Manchanda, R.; McGoron, A. J. *Appl. Biochem. Biotechnol.* **2011**, *165* (7−8), 1628−1651.
(9) Xie, J.; Chen, K.; Huang, J.; Lee, S.; Wang, J.; Gao, J.; Li, X.; Chen, X. *Biomaterials* **2010**, *31* (11), 3016−3022.
(10) Blanco, E.; Kessinger, C. W.; Sumer, B. D.; Gao, J. *Exp. Biol. Med.* **2009**, *234* (2), 123−31.
(11) Li, X.; Li, H.; Liu, G.; Deng, Z.; Wu, S.; Li, P.; Xu, Z.; Xu, H.; Chu, P. K. *Biomaterials* **2012**, *33* (10), 3013−3024.
(12) Cho, N. H.; Cheong, T. C.; Min, J. H.; Wu, J. H.; Lee, S. J.; Kim, D.; Yang, J. S.; Kim, S.; Kim, Y. K.; Seong, S. Y. *Nat. Nanotechnol.* **2011**, *6* (10), 675−82.
(13) Xuan, S. H.; Lee, S. F.; Lau, J. T.; Zhu, X.; Wang, Y. X.; Wang, F.; Lai, J. M.; Sham, K. W.; Lo, P. C.; Yu, J. C.; Cheng, C. H.; Leung, K. C. *ACS Appl. Mater. Interfaces* **2012**, *4* (4), 2033−40.
(14) Fernandez-Fernandez, A.; Manchanda, R.; McGoron, A. J. *Appl. Biochem. Biotechnol.* **2011**, *165* (7−8), 1628−51.
(15) Wen, H.-Y.; Dong, H.-Q.; Xie, W.-j.; Li, Y.-Y.; Wang, K.; Pauletti, G. M.; Shi, D.-L. *Chem. Commun.* **2011**, *47* (12), 3550.
(16) Dong, H.; Li, Y.; Cai, S.; Zhuo, R.; Zhang, X.; Liu, L. *Angew. Chem., Int. Ed. Engl.* **2008**, *47* (30), 5573−6.
(17) Bronich, T. K.; Keifer, P. A.; Shlyakhtenko, L. S.; Kabanov, A. V. *J. Am. Chem. Soc.* **2005**, *127* (23), 8236−8237.
(18) Lo, C.-L.; Lin, S.-J.; Tsai, H.-C.; Chan, W.-H.; Tsai, C.-H.; Cheng, C.-H. D.; Hsiue, G.-H. *Biomaterials* **2009**, *30* (23−24), 3961−3970.
(19) Torchilin, V. P. *J. Controlled Release* **2001**, *73* (2−3), 137−72.
(20) Jones, M.; Leroux, J. *Eur J Pharm Biopharm* **1999**, *48* (2), 101−11.
(21) Nasongkla, N.; Bey, E.; Ren, J. M.; Ai, H.; Khemtong, C.; Guthi, J. S.; Chin, S. F.; Sherry, A. D.; Boothman, D. A.; Gao, J. M. *Nano Lett.* **2006**, *6* (11), 2427−2430.
(22) Ebrahim Attia, A. B.; Ong, Z. Y.; Hedrick, J. L.; Lee, P. P.; Ee, P. L. R.; Hammond, P. T.; Yang, Y.-Y. *Curr. Opin. Colloid Interface Sci.* **2011**, *16* (3), 182−194.
(23) Kim, S. H.; Tan, J. P. K.; Nederberg, F.; Fukushima, K.; Yang, Y. Y.; Waymouth, R. M.; Hedrick, J. L. *Macromolecules* **2009**, *42* (1), 25−29.
(24) Glotzer, S. C.; Solomon, M. J. *Nat. Mater.* **2007**, *6* (8), 557−562.
(25) Li, G.; Shi, L.; Ma, R.; An, Y.; Huang, N. *Angew. Chem., Int. Ed.* **2006**, *45* (30), 4959−4962.
(26) Alexis, F.; Pridgen, E. M.; Langer, R.; Farokhzad, O. C. In *Handbook Experimental Pharmacology*; Springer: New York, 2010; Vol. *197*, pp 55−86.
(27) Zhang, G. D.; Zhang, R.; Wen, X. X.; Li, L.; Li, C. *Biomacromolecules* **2008**, *9* (1), 36−42.
(28) Xiao, Y.; Hong, H.; Javadi, A.; Engle, J. W.; Xu, W.; Yang, Y.; Zhang, Y.; Barnhart, T. E.; Cai, W.; Gong, S. *Biomaterials* **2012**, *33* (11), 3071−82.
(29) Hu, J.; Qian, Y.; Wang, X.; Liu, T.; Liu, S. *Langmuir* **2012**, *28* (4), 2073−2082.
(30) Liu, T.; Qian, Y. F.; Hu, X. L.; Ge, Z. S.; Liu, S. Y. *J. Mater. Chem.* **2012**, *22* (11), 5020−5030.
(31) Ren, T. B.; Liu, Q. M.; Lu, H.; Liu, H. M.; Zhang, X.; Du, J. Z. *J. Mater. Chem.* **2012**, *22* (24), 12329−12338.
(32) Xie, X. A.; Zhang, C. F. *J. Nanomater.* **2011**, No. 152524.
(33) Liu, T.-Y.; Liu, K.-H.; Liu, D.-M.; Chen, S.-Y.; Chen, I. W. *Adv. Funct. Mater.* **2009**, *19* (4), 616−623.
(34) Cohn, D.; Sagiv, H.; Benyamin, A.; Lando, G. *Biomaterials* **2009**, *30* (19), 3289−3296.
(35) O'Neil, C. P.; van der Vlies, A. J.; Velluto, D.; Wandrey, C.; Demurtas, D.; Dubochet, J.; Hubbell, J. A. *J. Controlled Release* **2009**, *137* (2), 146−151.
(36) Garinot, M.; Fievez, V.; Pourcelle, V.; Stoffelbach, F.; des Rieux, A.; Plapied, L.; Theate, I.; Freichels, H.; Jerome, C.; Marchand-Brynaert, J.; Schneider, Y. J.; Preat, V. *J. Controlled Release* **2007**, *120* (3), 195−204.
(37) Lin, J.-J.; Chen, J.-S.; Huang, S.-J.; Ko, J.-H.; Wang, Y.-M.; Chen, T.-L.; Wang, L.-F. *Biomaterials* **2009**, *30* (28), 5114−5124.
(38) Sone, E. D.; Stupp, S. I. *Chem. Mater.* **2011**, *23* (8), 2005−2007.
(39) Verbeeten, K. M.; Hermann, K. L.; Hasselqvist, M.; Lausten, G. S.; Joergensen, P.; Jensen, C. M.; Thomsen, H. S. *Eur. Radiol.* **2005**, *15* (1), 165−169.
(40) Bluemke, D. A.; Achenbach, S.; Budoff, M.; Gerber, T. C.; Gersh, B.; Hillis, L. D.; Hundley, W. G.; Manning, W. J.; Printz, B. F.; Stuber, M.; Woodard, P. K. *Circulation* **2008**, *118* (5), 586−606.
(41) Jaganathan, H.; Hugar, D. L.; Ivanisevic, A. *ACS Appl. Mater. Interfaces* **2011**, *3* (4), 1282−1288.